STRUCTURAL AND OPTICAL PROPERTIES OF SPUTTERED NANOCRYSTALLINE INDIUM NITRIDE ON SILICON SUBSTRATES

MARYAM AMIRHOSEINY

UNIVERSITI SAINS MALAYSIA

2013

STRUCTURAL AND OPTICAL PROPERTIES OF SPUTTERED NANOCRYSTALLINE INDIUM NITRIDE ON SILICON SUBSTRATES

By

MARYAM AMIRHOSEINY

Thesis submitted in fulfillment of the requirements for the degree of

Doctor of Philosophy

September 2013

ACKNOWLEDGMENTS

"All praises and thanks to ALLAH"

I would like to express my sincere appreciation and heartfelt thanks to my main supervisor, Professor Dr. Zainuriah Hassan, whose her expertise, guidance, and, understanding added considerably to my graduate experience. I wish to appreciate the persistent encouragement and support of my co- supervisor Dr. Sha Shiong Ng, for his guidance, time, comments, suggestions, and moral support throughout this project.

Great thanks for Universiti Sains Malaysia for providing me financial support for this research. Also, I would like to express my gratitude to the School of Physics, Universiti Sains Malaysia.

I would also like to express my appreciation to the staff in the Nano Optoelectronics Research Laboratory for their co-operation, technical assistance and valuable contribution to my work. The assistance from the staff of the Solid State Physics laboratory is also acknowledged.

Finally, words may not be sufficient to express acknowledgment to my parents, for their full support and encouragement. A special thanks to my lovely husband for which his patience and support were a powerful source in completing this study.

Maryam Amirhoseiny

Penang, Malaysia. March 2013

TABLE OF CONTENTS **Page**

ACKNOWLEDGEMENTS ii

TABLE OF CONTENTS iii

LIST OF TABLES x

LIST OF FIGURES xi

LIST OF SYMBOLS xvii

LIST OF ABBREVIATIONS xix

ABSTRAK xxi

ABSTRACT xxiii

CHAPTER 1 : INTRODUCTION

1.1. Introduction 1

1.2. Research objectives 4

1.2.1. Originality of the study 5

1.3. Outlines of the dissertation 5

CHAPTER 2: LITERATURE REVIEW AND THEORY

2.1. Introduction 7

2.2. III-nitride semiconductors 7

2.2.1. Fundamental properties of III-nitride semiconductors 7

2.2.2. Applications III-nitride semiconductors 10

2.2.3. Indium nitride 13

2.2.3.1. InN structural properties 13

2.2.3.2. InN electronic properties 14

2.2.3.3. InN optical properties 16

2.2.3.4. Review of InN growth history 18

2.2.3.5. RF magnetron sputtering (An alternative growth technique of nanocrystalline InN films) 21

2.3. Issues on the substrate for InN 23

2.3.1. Si as a suitable substrate for InN based devices 24

2.4. Principles of photo-electrochemical etching 26

2.5. Metal-semiconductor contacts theory 29

2.5.1. Band structures 29

2.5.2. Metal-semiconductor contacts 30

2.5.3. Schottky contact 31

2.5.4. Ohmic contact 34

2.6. Principles of InN-based photodetector devices 35

2.6.1. Photoconductor 35

2.6.2. PIN photodiode: 36

2.6.3. MSM photodetector 37

2.7. Summary 38

CHAPTER 3: METHODOLOGY AND EXPERIMENTAL EQUIPMENTS

3.1. Introduction 40

3.2. Growth of nanocrystalline InN 40

3.2.1 Preparation of substrates 40

3.2.2 Photo-electrochemical etching of Si (110) 43

3.2.3 RF sputtering system 44

3.3. Fabrication of devices 49

3.3.1 Metal coating tools 49

3.3.1.1 RF sputtering system 49

3.3.1.2 Thermal evaporator system 50

3.3.2 Thermal annealing processes 51

3.4. Structural characterization tools 52

3.4.1 X -ray diffraction 53

3.4.2 Scanning electron microscopy 56

3.4.3 Energy dispersive X-rays analysis 58

3.4.4 Atomic force microscopy 59

3.5. Optical characterization tools 60

3.5.1 Photoluminescence spectroscopy 60

3.5.2 Raman spectroscopy 62

3.5.3 FTIR spectroscopy 65

3.6. Electrical characterization tools 67

3.6.1 Current-voltage measurement equipment 67

3.6.2 Spectral responsivity equipment 68

3.7. Summary 69

CHAPTER 4 : RESULTS AND DISCUSSION (Part II):

STRUCTURAL, AND OPTICAL CHARACTERIZATIONS OF NANOCRYSTALLINE InN GROWN ON Si (110) SUBSTRATES

4.1. Introduction 70

4.2. Characterizations of InN samples grown on Si (110) at different RF powers 70

4.2.1. Scanning electron microscopy and energy dispersive X-ray analysis 70

4.2.2. Atomic force microscopy 73

4.2.3. X-ray diffraction 75

4.2.4. FTIR measurements 77

4.2.5. Raman measurements 78

4.3. Characterizations of InN samples grown on Si (110) at different gas ratios 79

4.3.1. Scanning electron microscopy and energy dispersive X-ray analysis 79

4.3.2. Atomic force microscopy 83

4.3.3. X-ray diffraction 84

4.3.4. FTIR measurements 85

4.3.5. Raman measurements 86

4.4. Characterizations of InN samples grown on Si (110) at different substrate temperatures 88

4.4.1. Scanning electron microscopy and energy dispersive X-ray analysis 88

4.4.2. Atomic force microscopy 89

4.4.3. X-ray diffraction 91

4.4.4. FTIR measurements 93

4.4.5. Raman measurements 94

4.5. Summary 95

CHAPTER 5: RESULTS AND DISCUSSION (Part III):

THE STUDY OF NANOCRYSTALLINE InN GROWN ON PHOTO-ELECTROCHEMICAL ETCHED Si (110) SUBSTRATES

5.1. Introduction 96

5.2. Photoelectrochemical etching under different etching times 96

5.2.1. Surface morphology 97

5.2.2. FTIR measurements 99

5.2.3. Photoluminescence measurements 100

5.2.4. Raman measurements 102

5.3. Photoelectrochemical etching under different current densities 103

5.3.1. FTIR measurements 103

5.3.2. Photoluminescence measurements 105

5.3.3. Raman measurements 106

5.4. Structural and optical characterization of nanocrystalline InN grown on photo-electrochemical etched Si (110) substrate 107

5.4.1. Scanning electron microscopy and energy dispersive X-ray analysis 108

5.4.2. X-ray diffraction 109

5.4.3. FTIR measurements 110

5.4.4. Raman measurements 111

5.4.5. PL measurements 112

5.5. Summary 115

CHAPTER 6 : RESULTS AND DISCUSSION (Part II):

COMPARISON OF STRUCTURAL AND OPTICAL CHARACTERIZATIONS OF NANOCRYSTALLINE InN GROWN ON DIFFERENT SUBSTRATES

6.1. Introduction 116

6.2. Comparison of structural and optical characteristic of InN thin films grown on Si (110), Si (100) and Si (111) substrates 116

6.2.1 Scanning electron microscopy and energy dispersive X-ray analysis 117

6.2.2 Atomic force microscopy 120

6.2.3 X-ray diffraction 120

6.2.4 FTIR measurements 123

6.2.5 Raman measurements 124

6.3. Comparison of structural and optical characteristic of InN thin films grown on Si (110) and SiC substrates 125

6.3.1 Scanning electron microscopy and energy dispersive X-ray analysis 126

6.3.2 Atomic force microscopy 128

6.3.3 X-ray diffraction 129

6.3.4 FTIR measurments 131

6.3.5 Raman measurements 132

6.3.6 PL measurements 133

6.4. Summary 134

CHAPTER 7: RESULTS AND DISCUSSION (Part IV):

FABRICATION AND CHARACTERIZATION OF InN-BASED PHOTODETECTORS

7.1. Introduction 136

7.2. InN- based photodetector 136

7.2.1. Ohmic contact 136

7.2.1.1. Effect of annealing temperature 136

7.2.1.2. I-V characteristic of InN photodetectors on different Si substrates 139

7.2.2. Schottky contact 141

7.2.2.1. Current-voltage measurements 141

7.2.2.2. Spectral responsivity measurements 144

7.3. Summary 145

CHAPTER 8: CONCLUSIONS AND FUTURE DIRECTION

8.1. Conclusions 147

8.2. Future direction 149

REFERENCES 151

LIST OF PUBLICATIONS 162

LIST OF TABLES

		Page
Table 2.1	Some of the important physical parameters of III-nitrides (Strite and Morkoc, 1992, Hsu et al., 2007, Bhuiyan et al., 2003, Chin et al., 1994, Mohammad and Morkoç, 1996).	11
Table 2.2	Lattice parameters, thermal expansion and surface energy of substrates.	26
Table 2.3	Electrical nature of ideal MS contacts.	30
Table 3.1	Operating conditions for deposition of nanocrystalline InN on Si (110) by the RF sputtering system.	48
Table 3.2	Operating conditions for deposition of nanocrystalline InN on different substrates by the RF sputtering system.	48
Table 3.3	Annealing conditions for the metal contacts.	52
Table 3.4	Raman active modes for hexagonal-InN at different geometry configurations.	64
Table 5.1	Full–width at half maximum (FWHM) of InN (101) diffraction peak, crystallite size, lattice constant, and the mismatch between InN and photo-electrochemical etched Si (110).	110
Table 6.1	Full–width at half maximum of InN (101) diffraction peak, crystallite size of InN films grown on different substrates, the mismatch between InN and different Si substrates and Si substrates surface energy.	123
Table 6.2	FWHM of InN (101) diffraction peak, crystallite size, lattice constant, and the mismatch between InN and different substrates.	130
Table 7.1	*I-V* characteristics of InN photodetectors in dark and under illumination.	144

LIST OF FIGURES

		Page
Fig. 1.1	Bandgap energies, E_g of the semiconductor materials (Kim, 2006).	1
Fig. 2.1	Different crystal structure of III-Nitrides; (a) wurtzite, (b) cubic zinc-blende, and (c) rock-salt.	8
Fig. 2.2	The wurtzite and zincblende crystal structures. (Bhatta, 2008)	15
Fig. 2.3	Photoluminescence spectra for MBE grown InN. (Davydov et al., 2002).	17
Fig. 2. 4	Bandgap energy for InN films as a function of carrier concentration. (Butcher & Tansley, 2005)	18
Fig. 2.5	Phase relations of InN shown by a decomposition curve separating InN and In+N_2 phase fields. Tetragons represent experimental conditions where metallic indium is observed. Shaded circles indicate that InN was stable. (Butcher & Tansley, 2005)	20
Fig. 2.6	Cubic crystalline structure of silicon.	24
Fig. 2.7	Common crystallographic planes.	25
Fig. 2.8	Diagram of the electronic band structure of metals, semiconductors and insulators. (Moller, 1993).	29
Fig. 2.9	Energy band diagrams for ideal MS contacts between a metal and a ntype semiconductor (a), (c) an instant after contact formation, and (b), (d) under equilibrium condition. (Sze & Ng, 2006)	31
Fig. 2.10	A metal n-type semiconductor pair (a) before and (b) after contact, with no surface/interface states. (Rhoderick & Williams, 1988)	32
Fig. 2.11	Plot of *ln I* as a function of V.	34
Fig. 2.12	Simple structure of photoconductors.	36
Fig. 2.13	Structure of a PIN photodetector.	37
Fig. 2.14	Structure of MSM photodetector.	38
Fig. 3.1	Flow chart of this research work.	41
Fig. 3.2	Schematic of wet etching set up.	44
Fig. 3.3	Schematic diagram of the RF magnetron sputtering system.	46
Fig. 3.4	Configuration of RF magnetron sputtering.	46

Fig. 3.5	Image of the RF sputtering equipment in the NOR Lab.	47
Fig. 3.6	Schematic of the InN photodetectors.	49
Fig. 3.7	Schematic diagram of thermal evaporator system.	50
Fig. 3.8	Image of the thermal evaporator in the NOR Lab.	51
Fig. 3.9	Schematic diagram of furnace for thermal annealing.	52
Fig. 3.10	Schematic collisions between X-ray beams and the atoms arranged in the lattice planes.	54
Fig. 3.11	Image of high resolution XRD equipments in NOR Lab.	56
Fig 3.12	Schematic of a SEM.	57
Fig. 3.13	Image of FESEM and EDX equipments in NOR Lab.	58
Fig. 3.14	Schematic figure of an AFM.	60
Fig. 3.15	Image of AFM, Bruker Dimension Edge equipment in NOR Lab.	60
Fig. 3.16	Radiative recombination paths: (a) band-to band; (b) donor to valence band; (c) conduction band to the acceptor. (d) Nonradiative recombination via an intermediate state. (Gfroerer, 2006)	61
Fig. 3.17	Schematic of PL setup.	62
Fig. 3.18	The schematic representation of the atom vibration modes. (Qian et al., 2004)	64
Fig. 3.19	Raman and PL system.	65
Fig. 3.20	Optical layout of a typical FTIR spectrometer. (Sun, 2009)	66
Fig. 3.21	Fourier transform IR spectrometer (Model Perkin Elmer Spectrum Gx).	67
Fig. 3.22	Current-voltage measurement system.	68
Fig. 3.23	A typical set up of spectral response measurements of the InN-based photodetectors	69
Fig. 4.1	SEM images of InN grown on Si (110) substrates with different RF powers.	71
Fig. 4.2	Atomic percentages of the In, N and O per unit surface of InN samples grown on Si (110) substrates with different RF powers.	72

Fig. 4.3	SEM cross section images of InN grown on Si (110) with different RF powers.	73
Fig. 4.4	AFM images of InN films grown on Si (110) with different RF powers.	74
Fig. 4.5	Effects of RF power on growth rate and RMS surface roughness of InN on Si (110) substrates.	75
Fig. 4.6	XRD spectra of diffraction peak of InN films on Si (110) as a function of RF power.	76
Fig. 4.7	Variations of FWHM of diffraction peak and crystallite size of InN films on Si (110) as a function of RF power.	77
Fig. 4.8	IR reflectance spectra of InN films grown on Si (110) substrates with different RF powers.	78
Fig. 4.9	Room temperature micro-Raman spectra of InN grown on Si (110) substrates with different RF powers.	79
Fig. 4.10	SEM images of InN grown on Si (110) substrates at different gas concentrations.	80
Fig. 4.11	SEM cross section images of InN grown on Si (110) substrates at different gas concentrations.	81
Fig. 4.12	Effects of gas concentrations on growth rate, resistivity and RMS surface roughness of InN on Si (110) substrates.	82
Fig. 4.13	Atomic percentages of the In, N and O per unit surface of InN samples grown on Si (110) substrates at different gas concentrations.	82
Fig. 4.14	AFM images of InN films grown on Si (110) substrates at different gas concentrations.	83
Fig. 4.15	XRD spectra of InN films grown on Si (110) as a function of gas concentrations.	84
Fig. 4.16	Variations of FWHM of diffraction peak and crystallite size of InN films grown on Si (110) as a function of gas concentrations.	85
Fig. 4.17	IR spectra of InN films grown on Si (110) substrates at different gas concentrations.	86
Fig. 4.18	Micro-Raman spectra of InN grown on Si (110) substrates at different gas concentration.	87

Fig. 4.19	SEM images of InN grown on Si (110) substrates at different substrate temperatures.	88
Fig. 4.20	Atomic percentages of the In, N, Si and O per unit surface of InN samples grown on Si (110) at different substrate temperatures.	89
Fig. 4.21	AFM images of InN films grown on Si (110) substrates at different substrate temperatures.	90
Fig. 4.22	XRD spectra of InN films grown on Si (110) as a function of substrate temperatures.	91
Fig. 4.23	Effects of substrate temperatures on resistivity, FWHM of XRD diffraction peak and crystallite size of InN films.	92
Fig. 4.24	IR spectra of InN films grown on Si (110) substrates at different substrate temperatures.	93
Fig. 4.25	Micro-Raman spectra of InN grown on Si (110) substrates at different substrate temperatures.	94
Fig. 5.1	(a) - (e) SEM images of photo-electrochemical etched Si (110) samples as a function of etching time.	98
Fig. 5.2	Anisotropy of silicon dissolution during the etching reaction (Langner, 2008).	99
Fig. 5.3	Schematic of the atomic arrangement of Si (110) plane. (Miyata and Kuroda, 1999)	99
Fig. 5.4	FTIR absorption spectra of photo-electrochemical etched Si (110) samples as a function of etching time.	100
Fig. 5.5	Photoluminescence spectra of photo-electrochemical etched Si (110) samples as a function of etching time.	101
Fig. 5.6	Raman spectra of photo-electrochemical etched Si (110) samples as a function of etching time.	102
Fig. 5.7	Transverse-optical (2TO) Raman phonon overtones of photo-electrochemical etched Si (110) samples as a function of etching time.	103
Fig. 5.8	FTIR spectra of photo-electrochemical etched Si (110) samples as a function of current density.	104
Fig. 5.9	Photoluminescence spectra of photo-electrochemical etched Si (110) samples as a function of current density.	105
Fig. 5.10	Raman spectra of photo-electrochemical etched Si (110) samples	106

as a function of current density.

Fig. 5.11 SEM images and (b) EDX results of InN thin films grown on PSi (110) layer. 108

Fig. 5.12 XRD spectrum of InN thin film grown on PSi (110) layer, the XRD spectrum of photo-electrochemical etched Si (110) is shown in the inset. 109

Fig. 5.13 FTIR absorption spectra of InN thin films grown on photo-electrochemical etched Si (110) layer. The inset shows the FTIR spectra for photo-electrochemical etched Si (110). 111

Fig. 5.14 Raman spectra of photo-electrochemical etched Si (110) sample and InN thin film grown on photo-electrochemical etched Si (110) layer. 112

Fig. 5.15 PL spectra of photo-electrochemical etched Si (110) sample and InN thin film grown on PSi layer. 113

Fig. 6.1 SEM images of InN grown on different orientations of Si substrates. 118

Fig. 6.2 SEM cross section images of InN grown on different orientations of Si substrates. 119

Fig. 6.3 Atomic percentages of the In, N and O per unit surface of InN samples grown on different orientations of Si substrates. 119

Fig. 6.4 AFM images of InN films grown on different orientations of Si substrates. 120

Fig. 6.5 XRD spectra of InN films on different orientations of Si substrates. 121

Fig. 6.6 IR spectra of InN films grown on different orientations of Si substrates. 124

Fig. 6.7 Micro-Raman spectra of InN grown on different orientations of Si substrates. 125

Fig. 6.8 (a,b) SEM images and (c, d) SEM cross section images of InN grown on Si (110) and 6H-SiC substrates, respectively. 126

Fig. 6.9: Atomic percentages of the In, N, Si and O per unit surface of InN samples grown on Si (110) and 6H-SiC substrates. 127

Fig. 6.10 AFM images of InN films grown on (a) Si (110) and (b) 6H-SiC substrates. 128

Fig. 6.11	XRD spectra of Nanocrystalline InN grown on Si (110) and 6H-SiC substrates.	129
Fig. 6.12	FTIR reflectance spectra of InN films grown on Si (110) and 6H-SiC substrates as measured at incident angle of 16°.	132
Fig. 6.13	Room temperature micro-Raman spectra of InN films grown on Si (110) and 6H-SiC substrates.	133
Fig. 6.14	PL spectra of InN films grown on Si (110) and 6H-SiC substrates.	134
Fig. 7.1	The I-V characteristics for InN photodetector under dark and illumination conditions: (a) as- grown, (b) annealed at 100 °C, (c) annealed at 200 °C, (d) annealed at 300 °C, and (e) annealed at 400 °C.	137
Fig. 7.2	Current–voltage characteristics for InN photodetector on (a) Si (110), (b) Si (100), and (c) Si (111) substrates under dark and illumination conditions.	140
Fig. 7.3	The gain values for InN photodetector on (a) Si (110), (b) Si (100), and (c) Si (111) substrates.	140
Fig. 7.4	Current–voltage characteristics for InN photodetector on Si (110) substrates at different annealing temperature.	142
Fig. 7.5	Responsivity of InN photodetector.	145

LIST OF SYMBOLS

a	Lattice constant
A	Area
A^{**}	Richardson's constant
c	Lattice constant
d	Interplanar spacing of the crystal planes
D	Average crystal size
E_C	Conduction band
E_F	Fermi level of semiconductor
E_g	Semiconductor band gap
E_v	Valence band edge
(hkl)	Miller indices
I	Current
I_o	Saturation current
J	Current density
k	Boltzmann constant
m_o	Electron mass
m^*	Effective mass
m_n	Electron effective mass
m_p	Hole effective mass
Nc	Effective density of states
n	ideality factor
n	Free electron concentration
p	Free hole concentration
P	Porosity

q	Electron charge
R	Responsivity
R	Resistance
T	Thickness
t	Time
T	Absolute temperature
V	Voltage
α	Absorption coefficient
ε_a	Strain along a-axis
ε_c	Strain along c-axis
σ	Conductivity
θ	Incident / diffraction angle
χ	Semiconductor electron affinity
φ_B	Schottky barrier height
ϕ_M	Metal work function
ϕ_S	Semiconductor work function
μ_n	Electron mobility
μ_p	Hole mobility
μ	Effective dipole moment
ρ	Resistivity
λ	Wavelength
η	Quantum efficiency

LIST OF ABBREVIATIONS

a.u.	Arbitrary unit
AFM	Atomic force microscopy
AlN	Aluminum nitride
Ar	Argon
BL	Blue luminescence
CB	Conduction band
DC	Direct current
ECD	Electrochemical deposition
EDX	Energy dispersive X-ray
eV	Electron volt
FTIR	Fourier transform infrared
FWHM	Full width at half maximum
GaAS	Gallium arsenide
GaN	Gallium nitride
HF	Hydrofluoric acid
In	Indium
IR	Infrared
I-V	Current-voltage
LD	Laser diode
LED	Light emitting diode
LO	Longitudinal optic
MgO	Magnesium oxide
M	Metal
MBE	Molecular beam epitaxial

MESFET	Metal-semiconductor field effect transistor
MOCVD	Metalorganic vapor deposition
MS	Metal semiconductor
MSM	Metal semiconductor metal
N_2	Nitrogen
O.T	Optical transmission
PC	Photocurrent
PECE	Photoelectrochemical etching
PL	Photoluminscence
Pt	Platinum
RMS	Root mean square
SBH	Schottky barrier height
SC	Semiconductor
sccm	Standard cubic centimeters per minute
SEM	Scanning electron microscopy
Si	Silicon
TO	Transverse optic
UV	Ultra violet
VB	Valence-band
VIS	Visible
XRD	X-ray diffraction
WZ	Wurtzite structure
ZB	Zinc blend structure

SIFAT STRUKTUR DAN OPTIK INDIUM NITRIDA BERHABLUR NANO YANG DIPERCIKKAN ATAS SUBSTRAT SILIKON

ABSTRAK

Tujuan projek ini adalah untuk mengkaji penumbuhan dan pencirian indium nitrida (InN) berhablur nano atas substrat silikon (Si) dengan menngunakan pelbagai pencirian yang tidak bersentuh dan tidak membinasakan. Ini termasuk mikroskop imbasan elektron, analisis tenaga serakan sinar-X, mikroskop daya atom, dan pembelauan sinar-X untuk pencirian struktur, dan spektroskopi jelmaan Fourier inframerah, spektroskopi mikro Raman, dan spektroskopi fotoluminesen untuk pencirian optik.

Kerja-kerja awal pada pencirian struktur dan optik InN berhablur nano yang ditumbuhkan atas orientasi anisotropik (110) bagi substrat silikon (Si) telah dijalankan. Kajian bagaimanapun memberi tumpuan kepada mengoptimumkan keadaan pemendapan bagi penumbuhan InN berhablur nano menggunakan kaedah percikan frekuensi radio. Semua filem yang dimendapkan yang diperolehi di bawah keadaan yang berbeza adalah sedikit kaya-nitrogen, tetapi peningkatan kuasa percikan frekuensi radio memberikan lebih sebatian InN dalam bentuk stoikiometri. Keputusan pembelauan sinar-X mendedahkan filem wurtzit InN berhablur nano dengan orientasi pertumbuhan diutamakan (101) untuk semua filem yang dimendapkan. Puncak spektroskopi fotoluminesen yang kuat diperhatikan dalam tenaga sebanyak 1.9 eV pada suhu bilik. Nilai yang lebih tinggi bagi jurang jalur adalah disebabkan oleh anjakan Moss-Burstein.

Parameter pemendapan percikan yang optimum bagi InN yang ditumbuhkan atas substrat Si (110) telah digunakan sebagai latar belakang untuk mengkaji pemendapan InN pada substrat yang berbeza seperti Si (110) yang dipunarkan secara

foto-elektrokimia, orientasi berbeza substrat Si, dan substrat 6H-silikon karbida. Maksimum separuh lebar penuh yang terendah (0.246°) dan saiz hablur tertinggi (42.3nm) bagi InN berhablur nano yang ditumbuhkan atas Si (110) mendedahkan bahawa filem-filem InN yang tumbuhkan pada Si (110) anisotropik mempunyai struktur hablur nano terbaik berbanding dengan orientasi substrat Si yang lain. Dalam kes substrat 6H-silikon karbida, kehabluran filem InN menurun berbanding dengan yang ditumbuhkan atas Si (110). Keputusan pembelauan sinar-X mendedahkan ketidaksepadan kekisi yang besar (sekitar 6.2%) di antara InN (101) dan 6H-silikon karbida yang merupakan sebab utama bagi terikan yang besar dalam filem-filem yang dimendapkan dan dengan itu mengurangkan kualiti hablur.

Akhirnya, pengesan foto berasaskan InN telah difabrikasikan. Sentuhan ohmik argentum (Ag) dan sentuhan Schottky platinum (Pt) dimendapkan dengan menggunakan corak topeng logam-semikonduktor-logam. Pengesan foto InN disepuh lindap pada suhu yang berbeza (100-400°C) dalam persekitaran N_2 untuk melegakan tegasan dan untuk mengaruhkan tindak balas yang menggalakkan antara logam dan semikonduktor. Pengukuran arus-voltan selepas rawatan haba telah dilakukan dalam keadaan gelap dan pencahayaan. Gandaan yang diperolehi dalam peranti-peranti ini telah didapati sangat bergantung pada orientasi Si. Nilai tertinggi gandaan (1.9) untuk voltan malar 3 V telah dicapai bagi pengesan foto InN atas Si (110). Ketinggian sawar dan faktor keunggulan pengesan foto didapati bergantung kepada suhu. Ketinggian sawar paling rendah (0.60 eV) dan faktor keunggulan (1.015) telah diperolehi daripada arus foto pengesan foto InN yang disepuh lindap pada 400°C.

STRUCTURAL AND OPTICAL PROPERTIES OF SPUTTERED NANOCRYSTALLINE INDIUM NITRIDE ON SILICON SUBSTRATES

ABSTRACT

The aim of this project is to study the growth and characterization of nanocrystalline indium nitride (InN) on silicon (Si) substrates by means of various non-contact and non-destructive characterization tools. These include the scanning electron microscopy (SEM), energy dispersive X-ray (EDX) analysis, atomic force microscopy (AFM), and X-ray diffraction (XRD) for structural characterization, and Fourier transform infrared (FTIR) spectroscopy, micro-Raman spectroscopy, and photoluminescence (PL) spectroscopy for optical characterization.

Initial works on the structural and optical characterization of the nanocrystalline InN grown on anisotropic (110) orientation of sillicon (Si) substrates have been carried out. Studies are, however, focused on optimizing the deposition conditions for growing nanocrystalline InN by radio frequency (RF) sputtering method. All deposited films obtained under different deposition conditions were slightly nitrogen-rich, but increasing the RF power provided more InN compounds in stoichiometric form. XRD results revealed wurtzite nanocrystalline InN films with a (101) preferred growth orientation for all deposited films. The strong PL peak was observed in the energy of 1.9 eV at room temperature. This higher value of the bandgap is due to the Moss–Burstein shift effect.

The optimized sputtering deposition parameters for InN grown on Si (110) substrates were used as background to study the deposition of InN on different substrates such as photo-electrochemical etched Si (110), different orientations of Si substrates, and 6H-silicon carbide (6H-SiC) substrates. Lowest full width at half maximum (FWHM) (0.246°) and highest crystallite size (42.3nm) of nanocrystalline

InN grown on Si (110) reveal that InN films which grew on anisotropic Si (110) has the best nanocrystallite structure as compared to other orientation of Si substrates. In the case of the 6H-SiC substrate, the crystallinity of InN films degraded as compared to that grown on Si (110). The XRD result revealed a large lattice mismatch (around 6.2%) between InN (101) and 6H-SiC which is the main reason for the large strain in the deposited films and thus reduces the crystalline quality.

Finally, InN based photodetectors were fabricated. Silver (Ag) ohmic and platinum (Pt) Schottky contacts were deposited by using a metal-semiconductor-metal (MSM) pattern mask. The InN photodetectors were annealed at different temperatures (100-400°C) in an N_2 environment to relieve stress and to induce any favorable reactions between the metals and the semiconductors. Current-voltage (I-V) measurements after heat treatment were performed in the dark and illuminated conditions. The gain obtained in these devices has been found to depend strongly on the Si orientations. The highest gain value (1.9) for a constant voltage of 3 V was achieved for InN photodetectors on Si (110). The barrier height and ideality factor of the photodetectors were found to be temperature dependent. The lowest barrier height (0.60 eV) and ideality factor (1.015) were obtained from photocurrent of InN photodetectors annealed at 400°C.

CHAPTER 1

INTRODUCTION

1.1. Introduction

Gallium nitride (GaN), aluminum nitride (AlN), indium nitride (InN), and their alloys represent the family of III-nitride semiconductors. In recent years, the group III-nitrides have been strongly studied due to their inherent potential for photovoltaics, high efficiency solid-state lighting, high power and temperature electronics (Veal et al., 2009). The general inherit characteristics of these materials including physical hardness, chemical inertness and wide bandgap, make III-nitrides compounds as the promising materials for semiconductor device applications where conventional III-V semiconductor materials are not capable to use (Ambacher, 1999). The bandgaps of III-nitride materials can be adjusted from near infrared (0.7 eV, pure InN) to ultraviolet (6.2 eV, pure AlN). The bandgap energies of the semiconductor materials are shown in Fig.1.1 (Kim, 2006).

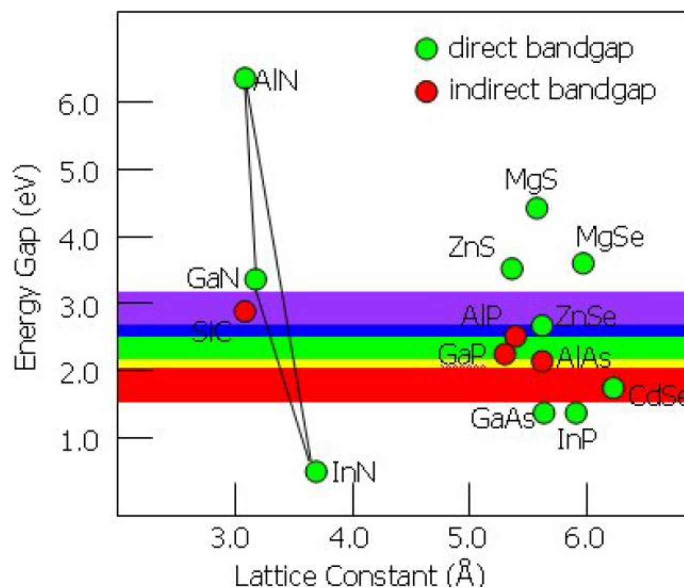

Fig. 1.1: Bandgap energies, E_g of the semiconductor materials (Kim, 2006).

InN has a wurtzite crystal structure with a bandgap ranging from 0.7 eV to 1.9 eV (Butcher and Tansley, 2005). InN is an interesting semiconductor material among other III-nitrides because of its small energy bandgap, smallest effective mass, high electron mobility, and the highest electron drift velocity. Due to these special characteristics, its may be used in high frequency and high power optoelectronic devices, such as high efficiency solar cells, high electron mobility sensors, and transistors (Feng et al., 2012; Nguyen et al., 2011; Lai et al., 2010; Miller et al., 2010).

The low energy optical response and high absorbance of InN makes it a promising candidate for multi-junction, and high-efficient solar cells (Wu et al., 2003). However, InN has received less attention compared with GaN and AlN primarily because of difficulties inherent in the preparation of its stoichiometric form (Motlan et al., 2002). In addition, high-grade single crystal InN is difficult to grow due to its low dissociation temperature (Guo et al., 1993) and less suitable substrates. Owing to its low dissociation temperature, InN film should be deposited at low temperatures to avoid nitrogen (N) atom re-evaporated. Reactive sputtering is one of the most promising techniques of producing InN from the viewpoint of low-temperature film growth. Apart from that, the fundamental characteristics of InN are being highly debated. Arguments surround the InN material in terms of its energy bandgap, variation of the decomposition temperature, defect properties, electron effective mass, the role of oxygen, and suitable substrates.

InN films have a large concentration of dislocations and defects which make some limitations in InN-based optical devices. The bandgap of InN films is strongly dependent on their growth conditions. Until 2001, it was generally accepted that InN had a bandgap of about 1.89 eV at room temperature, from early studies of

polycrystalline InN films (Tansley and Foley, 1986). A few years ago more serious efforts to grow single crystalline InN films with MBE were undertaken (Davydov et al., 2002b), and studies of such material lead to a sudden revision of the lowest bandgap down to about 0.7 eV (Butcher and Tansley, 2005; Davydov et al., 2002a; Li et al., 2011). Various factors that contribute to variations in bandgap include Moss–Burstein energy shifts (Chakraborty et al., 2003), the presence of oxide precipitates (Davydov et al., 2002a), the polycrystalline nature of the sample, and other stoichiometry-related defects (Butcher and Tansley, 2005; Li et al., 2011). The Moss–Burstein shift effect occurs when the carrier concentration exceeds the conduction band edge density of states and the Fermi level is positioned within the conduction band (Chakraborty et al., 2003). However, these effects have not been clearly elucidated, and the stoichiometry between indium (In) and N in InN films remains an important dispute. Previously, InN was assumed to be unable to grow nitrogen-rich because InN growth under thermal equilibrium conditions is not possible to be nitrogen-rich (Miller et al., 2010). On the other hand, in radio frequency (RF) sputtering, the use of plasma sources of nitrogen creates non-equilibrium growth regimes. Large variations in bandgap may be attributed to changes in material stoichiometry, thus requiring further investigation. One critical issue in InN research is that the films grown by different techniques frequently show different characteristics.

InN layer synthesis on sapphire and glass substrates using reactive sputtering has been previously reported (da Silva et al., 2012; Takai et al., 1998; Inoue et al., 2004), and InN deposition on different Si substrate orientations has been recently investigated (Cai et al., 2009). The anisotropic Si (110) surface offers a unique orientation for III-nitride films, decreasing the defect density and tensile stress for

film cracking (Cordier et al., 2009). However, to the best of our knowledge, the growth of nanocrystalline InN on Si (110) has not been explored. Si (110) is a surface orientation generally used in Si technology, and the growth of nanocrystalline InN on such substrates should be suitable for future III-N device integration.

1.2. Research objectives

The primary objective of this project is to study the structural, optical and electrical properties of nanocrystalline InN grown on Si substrates using radio frequency sputtering (RF sputtering). Growth processes and structures will be investigated using a variety of post deposition analysis tools including high resolution X-ray diffraction (HR-XRD), scanning electron microscopy (SEM), energy dispersive X-ray spectroscopy (EDX), atomic force microscopy (AFM), Fourier transform infrared (FTIR) spectroscopy, micro-Raman and photoluminescence (PL) spectroscopy. These characterization techniques will provide information such as crystalline quality, composition, lattice parameters, layer thickness, material density, interface roughness, stress/strain, crystallite size, and defects in the grown layers.

The second objective is to synthesize the photo-electrochemical etched Si layers prepared on n-type (110) oriented Si and use it as an inner layer to fabricate InN/ photo-electrochemical etched Si/Si (110) heterostructure.

The third objective is to investigate and compare the main structure and optical characteristics of the nanocrystalline InN grown on Si (110) and other substrates. The nanocrystalline InN were deposited onto different crystalline

orientation of Si as well as 6H-silicon carbide (6H-SiC) substrates using RF reactive magnetron sputtering at room temperature.

The fourth objective is to fabricate metal-semiconductor-metal (MSM) photodetector based on the nanocrystalline InN thin films on Si substrates. In this work, the ohmic and Schottky contacts were deposited via RF reactive magnetron sputtering and thermal vacuum evaporation on nanocrystalline InN and the current-voltage (I-V) characteristics were investigated.

1.2.1. Originality of the study

The main originality of this study lies in achieving a good stoichiometry nanocrystalline InN layers with good crystalline quality on (110) crystalline orientation of Si substrate by radio frequency (RF) sputtering method. Secondly, photo-electrochemical etched Si layers were synthesized on n-type (110) oriented Si. The InN/photo-electrochemical etched Si (110) heterostructure was successfully fabricated at room temperature. In addition, a comprehensive study revealed that (110) is the best orientation for Si substrates to grow nanocrystalline InN. Finally, the MSM photodetectors which can work in IR range have been fabricated

1.3. Outlines of the thesis

Generally, the contents of this dissertation are organized as follows.

Chapter Two presents some detailed review on structural, optical and electrical properties of InN materials. In addition, a brief description on deposition techniques of nitride thin films, especially RF sputtering method is given. The discussion also covers the motivation for choosing Si (110) as a suitable substrate for

InN based devices. In addition, we discuss the metal-InN contact technology, and the relevant concepts of Ohmic and Schottky contacts.

Chapter Three covers the basic concepts of the growth of InN by a typical sputtering system. In addition, the sample preparation of the InN heterostructures with various growth conditions is described. After that, the basic principles of characterization tools which were used in this study are also presented.

Chapter Four presents and discusses the structural and optical characteristics results of nanocrystalline InN thin films grown on Si (110) at different growth conditions. It is divided into three main sections, i.e., characterization of InN samples grown at different RF powers, gas ratio and substrate temperatures.

Chapter Five discusses the photo-electrochemical etching of the Si (110) substrates. The effects of etching time and etching density on surface morphology and optical properties of silicon (110) were reported. Furthermore the structural and optical characteristics of nanocrystalline InN on photo-electrochemical etched Si (110) were presented.

Chapter Six presents and discusses the effects of different substrates on the structural and optical characteristics of InN thin films.

Chapter Seven discusses the results of metal contacts. The effects of annealing temperature on Ohmic and Schotky contacts were given. In addition, the effects of Si substrate orientations on I-V characteristics of InN- based devices were described in this chapter.

Finally, **Chapter Eight** presents the conclusions and future works.

CHAPTER 2

LITERATURE REVIEW AND THEORY

2.1. Introduction

III-nitride semiconductors have a wurtzite crystalline structure and a direct wide energy bandgap from 0.7 eV for InN to 6.2 eV for AlN. In recent years, the III-nitride semiconductors, InN, GaN, AlN, and their ternary alloys have attracted lots of attention. This is due to their intrinsic properties such as, thermal and chemical stability, high thermal conductivity, direct wide energy bandgap, high acoustic wave velocity and low compressibility (Khoshman, 2005). The III nitrides are also very promising materials for high efficiency optoelectronic devices and high temperature/power electronic devices. This chapter begins with a brief review of III-nitride properties and applications. After that, issues on fundamental properties of InN are discussed and followed by a review of the growth history of InN. RF sputtering method which is used in this study to grow crystalline InN will be explained. In addition, issues on the substrate for InN will be discussed briefly. Since photo-electrochemical etched Si (110) was used as a substrate for the growth of nanocrystalline InN in this research, the principles of photo-electrochemical etching will be expressed. Finally, the essential theories of metal-semiconductor (MS) contacts and also principles of InN-based photodetector devices are described.

2.2. III-nitride semiconductors

2.2.1. Fundamental properties of III-nitride semiconductors

III-nitride compound semiconductor is formed when an element from the group III like boron, gallium, indium or aluminum is bonded with the nitrogen in

group V. GaN, AlN, and InN are the common III-nitrides semiconductors currently being studied. These III-nitride compounds are mostly covered by covalent chemical bonds. They are found to have the following three structural crystalline phases; zincblende, wurtzite and rock-salt, as shown in Fig. 2.1.

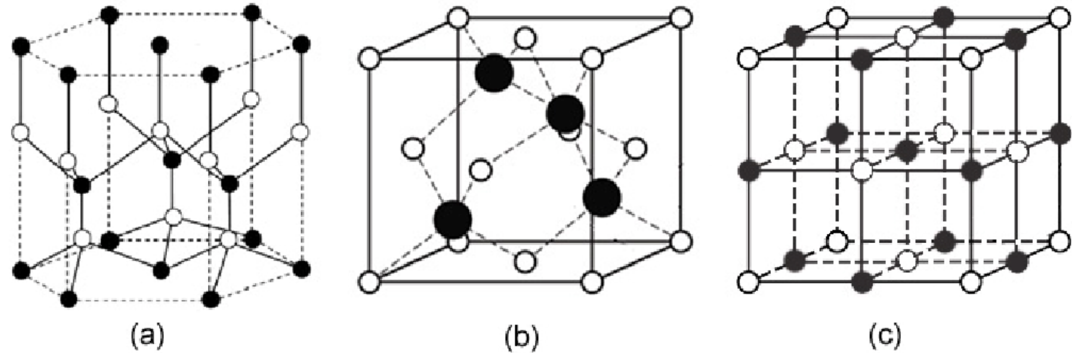

Fig. 2.1: Different crystal structures of III-nitrides; (a) wurtzite, (b) cubic zinc-blende, and (c) rock-salt. (Ye, 2011)

At ambient conditions, wurtzite structure is the thermodynamically stable phase (Meng and Edgar, 1994). The zincblende crystalline structure is metastable and by growing the heteroepitaxial thin film on cubic structures such as gallium arsenide (GaAs), magnesium oxide (MgO) and silicon (Si) (Gil, 1998) with (001) crystal planes, it can be stabilized. A rock-salt structure can be achieved at high pressure (Gil, 1998). The zincblende and wurtzite structures are quite similar in some aspects. In both of them, the element of group III is surrounded with four atoms from the group V element and the element of group V is surrounded with four atoms from group III elements, as well. In addition, the twelve next nearest neighbours are at the same distance in both structures. It is found that third next nearest neighbours are the main difference of zincblende and wurtzite structure, as they have difference in their stacking sequences. The stacking sequence of the zincblende structure along [001]

direction is ABCABC while that of wurtzite structure along [0001] is ABAB, while A, B, and, C can be referred to allowed sites of the III-nitride pairs of closed-packed layers. A stacking fault might transform a structure to another one or creates a structural defect.

GaN, AlN, InN and their ternary or quaternary alloys such as (InGaN, InAlN, and AlGaN or AlGAInN) are direct bandgap semiconductors which cover the spectral range of 0.7 eV for InN (near infrared) to 6.2 eV for AlN (deep ultraviolet). However, an argument exists concerning the energy band gap of InN.

AlN shows many practical properties that make it functional for interesting electronic applications such as high thermal conductivity, its hardness, and resistance to high temperature and caustic chemicals. Because of the high resistivity and wide bandgap, undoped AlN exhibits insulating behavior. Consequently, AlN is not the easy substance to study. Due to the reactivity of the Al, high purity source and an oxygen-free atmosphere is needed to grow good quality AlN. Recently with the accessibility of refined growth methods, AlN is grown with a high crystal quality, and exhibits both p- and n-type conduction. GaN is one of the top lists of studies among group III-nitrides which is important material in the optoelectronic technology. Undoped GaN always exhibits unintentional n-type characteristic. Growth of the p-type GaN has directed researchers to reveal excellent p-n junction LEDs which are able of working in a variety of wavelength regimes.

Electronic properties, mobility and carrier concentration are the essential factors affecting the efficiency and performance of electronic devices. Carrier mobility depends on various factors, such as material quality, electric field, temperature and doping concentration of the semiconductors. The higher lattice mismatch causes the lower value of carrier mobility. By utilizing a buffer layer

through the deposition, the strain reduces and the carrier mobility enhances. Because of the low carrier concentrations (less than 10^{16} cm^{-3}), the evaluated electrical properties such as impurities and native defects of the AlN semiconductor are limited to resistivity measurements. The reported value for the electron concentration of undoped GaN samples at room temperature are around 10^{16} cm^{-3} and the mobility about 1000 $cm^2V^{-1}s^{-1}$ while for InN are in the order of 10^{18} cm^{-3} and 4000 $cm^2V^{-1}s^{-1}$, respectively (Mohammad and Morkoç, 1996). The structural and optical properties of InN are discussed later. Dielectric constants and refractive index of the semiconductors are the factors effect on the optical characteristics of devices. Some of the structural, optical, electronic, and thermal properties of wurtzite GaN, AlN, and InN are summarized in Table 2.1.

2.2.2. Applications of III-nitride semiconductors

III-nitride semiconductors compound have been strongly studied in last two decades due to their potential applications in optoelectronic, electronic device structures. The recent findings demonstrate that III-nitride based semiconductors are capable for nanostructured materials. Using the GaN, AlN and their alloys in the optical devices, can be extended to the blue range and beyond for the electronics functioning at high temperatures and also caustic environment. Because of the wide bandgap of AlN and low bandgap of InN, the compounds of GaN with In and Al can fabricate the wide variety of the energy bandgaps from 0.7 eV (near infrared) to 6.2 eV (deep ultraviolet regime).

Table 2.1: Some of the important physical parameters of III-nitrides (Bhuiyan et al., 2003, Chin et al., 1994, Hsu et al., 2007, Mohammad and Morkoç, 1996, Strite and Morkoc, 1992).

Parameter	**GaN**	**AlN**	**InN**
Lattice constant, a (Å)	3.189	3.112	3.545
Lattice constant, c (Å)	5.186	4.982	5.703
Energy gap (pure material) (eV)	3.4	6.2	0.7
Thermal conductivity (W/cm K)	1.3	2.0	-
Electron effective mass, $m^*_c(m_o)$	0.2	0.4	0.11
Heavy hole effective mass, $m^*_{hh}(m_o)$	0.8	3.5	1.6
Mobility electrons (cm^2/Vs), 300K	≤1000	≤300	≤3200
Peak drift velocity (cm/s)	3.1×10^7	1.7×10^7	5×10^7
Dielectric constant, (ε_o)	8.9	8.5	15.3
Mass Density (g/cm^3)	6.09	3.23	6.81
Deformation potential (eV)	9.1	9.5	3.6

The fabrication of hetero and homojunction GaN based devices propelled to commercialization of laser diodes and light emitting diodes (Pankove and Moustakas, 1998). The commercial and practical applications of these GaN based materials can be utilized in back lighting of mobile phones, traffic lights , indoor lights, light indicators of electronic devices, solid state lasers, and high power microwave transistors. Even though GaInN-based lasers diodes, LEDs and microwave transistors are developed and commercialized, but the potential application of GaN- based alloys for the high temperature and high power transistors and other optoelectronic devices are still being researched. InN and AlN are still less

studied for commercial device. Due to the wide bandgap of GaN and AlN, these are capable materials to fabricate the UV emitters and detectors. III-nitrides based UV emitters can be applied for material identification, curing, forensic location, and also material processing applications. III-nitrides based UV detectors are used in the UV sensing applications like vehicle engine combustion sensing, high temperature flame sensing, burner monitoring into the gas turbines, solar blind detectors, environmental monitoring, remote sensing of the earth resources. Developed group III-nitride based materials will offer a basis for the novel devices that are important significantly for space exploration missions because of their strength against radiation damage. The wide bandgap of III-nitrides and their strong bond force (2.2, 2.88 and 1.93 eV/bond for GaN, AlN and InN, respectively) (Harrison, 1989) make them resistant to the radiation damage. In addition, high dissociation temperature and high melting point of AlN and GaN make them capable materials for high power and, high temperature transistors. III-nitride materials also can be used into the terahertz (THz) device structures. Meziani *et al.*(Meziani et al., 2005) have studied the optical characterization of InN samples in the THz range and then concluded that InN can be a great interest for recognition of terahertz devices because of its high electron velocity, which is higher than those in InAs and GaAs.

Fabrication of quantum infrared (IR) detectors is another essential application of III-nitride based semiconductors. Photoconductors are one of the most common types of quantum IR detectors that can be fabricated based on nitride semiconductors. InN based semiconductor can be suitable substances for photovoltaic applications due to the small bandgap of InN. A single chip of $In_xGa_{1-x}N$ can absorb the whole visible range of the solar radiation and then result in highly performance solar cells. In addition, transistors, LEDs, and laser diodes usually

involve $In_xGa_{1-x}N$, with low indium fractions. Therefore, there would be lots of advantages in being capable to include large indium fractions in different device applications. For example, using the wurtzite $In_xGa_{1-x}N$ with low gallium fraction would lead photonic devices in the red wavelength area and much faster electronic devices, due to higher mobility and peak velocity than found in most of the other III-nitride materials (Bhuiyan et al., 2003). The potential of extending the energy bandgap of group III-nitride based semiconductors to the near infrared spectral area has created considerable interest and also extensive researches have been initiated. The characteristics and potential applications of InN in various areas have been reported (Alevli et al., 2008, Butcher and Tansley, 2005, Davydov et al., 2002b, Lai et al., 2010, Maleyre et al., 2004, Nguyen et al., 2011). A brief summary of characteristics and applications of InN are expressed in the following section.

2.2.3. Indium nitride

2.2.3.1. InN structural properties

Characterization of the crystal structure of the InN is essential in order to select a suitable substrate and optimizing the disposition condition to achieve high quality InN thin films. XRD is a nondestructive technique which discovers detailed information about the crystallographic structure and chemical composition of any materials. By using the structural characterization techniques, it has been found that the crystalline InN can have three different structures, zincblende, wurtzite, and rock salt, similar to those of other nitrides.

Thermodynamically, the hexagonal wurtzite structure is the most stable crystal structure. However, InN can be achieved in the cubic zincblende structures as well when grown on (001) crystal planes of cubic substrates such as Si and GaAs.

The wurzite structure has a hexagonal unit cell and hence two lattice constants *a* and *c*. It includes six atoms of each indium and nitrogen. The zincblende structure has a cubic unit cell with a lattice constant of *a*, including four atoms of each indium and nitrogen. In both hexagonal and cubic crystalline structures, every nitrogen atom is coordinated by four indium atoms and every indium atom are coordinated by four nitrogen atoms as shown in the Fig. 2.2 (Bhatta, 2008). The lattice constant values (*a* and *c*) of InN might be effected by the growth conditions, the film stoichiometry, and impurity concentrations. Juza and Hahn (Juza and Hahn, 1938) was the first who reported the wurtzite structure of InN with lattice parameters c = 5.69 Å, and a = 3.53 Å. These values are close to c = 5.7600 Å, a = 3.5480 Å and c =5.7083 Å, a = 3.5390Å reported by Tansley & Foley (T. L. Tansley, 1985), and Maleyre et al. (Maleyre et al., 2004), respectively.

2.2.3.2. InN electronic properties

The carrier concentration and mobility values of first polycrystalline InN thin films grown by radio frequency (RF) sputtering of metallic indium in a nitrogen atmosphere were reported in the range of 10^{18} cm^{-3} and 250 $cm^2V^{-1}s^{-1}$, respectively (Hovel and Cuomo, 1972). Later Tansley and Foley, have presented carrier concentrations around 10^{16} cm^{-3} and high mobility about 3980 $cm^2V^{-1}s^{-1}$ (Tansley and Foley, 1984). However, Scott *et al.* (Scott et al., 2001) applied the same method and expressed carrier concentrations in the range of 10^{19} cm^{-3} and mobility less than 100 $cm^2V^{-1}s^{-1}$, which are in a good agreement with the reported values for polycrystalline samples.

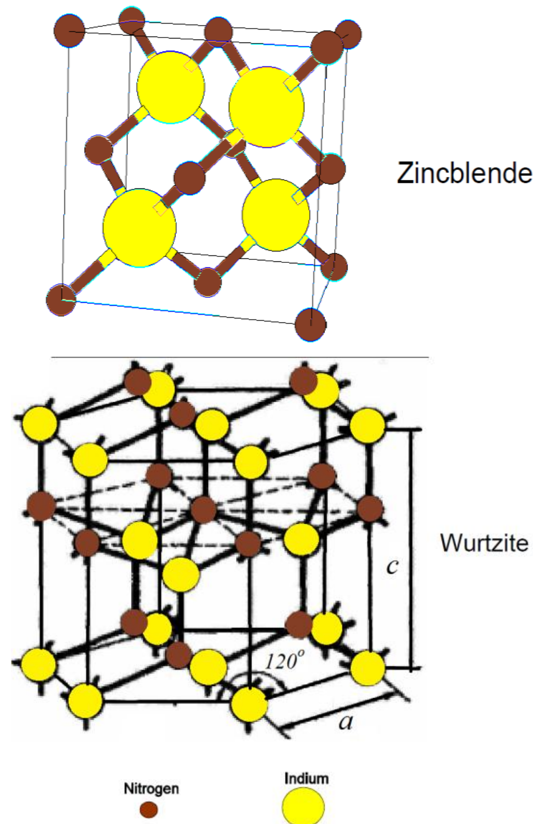

Fig. 2.2: Wurtzite and zincblende crystal structures for InN. (Bhatta, 2008)

Tansley and Foley have reported that the energy bandgap of InN sample is around 1.89 eV which was generally accepted until near 2002 (Tansley and Foley, 1986). However, based on optical absorption, photoluminescence (PL) measurements carried out on InN samples grown by MBE (with having low electron concentrations), the energy gap of InN has been achieved around 0.7 eV (Briot et al., 2004, Butcher and Tansley, 2005, Higashiwaki and Matsui, 2003). For the MBE grown InN samples, the lowest carrier concentration value was reported around 10^{17} cm^{-3} and the highest mobility value was 2200 $cm^2V^{-1}s^{-1}$ (Swartz et al., 2004). This explanation of PL and optical absorption data of InN bandgap has been discussed by Shubina *et al.*(Shubina et al., 2004). They claimed that the energy bandgap of the InN samples is much wider than the newly accepted value. According to their description, the lower absorption edge of InN sample is because of Mie scattering

effect by metallic indium clusters and the achieved PL peak at 0.7 eV in InN initiates from optical transitions implicating interface states between the indium nitride matrix and the indium clusters. The details about optical properties and energy bandgap of InN will discuss in following section.

2.2.3.3. InN optical properties

Until 2002, the measured energy bandgap of 1.89 eV has been accepted for InN (Tansley and Foley, 1986). However, several groups after that showed the energy bandgap of InN is in between 0.7 and 0.90 eV, (Briot et al., 2004, Butcher and Tansley, 2005, Davydov et al., 2002b, Higashiwaki and Matsui, 2003) which is quite smaller than 1.89 eV.

Evidence of a small energy bandgap for InN was presented in 2001. Inushima *et al*. reported that the absorption edge of the InN grown by MBE lies near 1.1 eV, that is much lower than the previously reported values (Inushima et al., 2001). Davydov *et al*. showed an energy bandgap value around 0.9 eV for high quality InN layer grown by MBE, by means of photoluminescence excitation (PLE) spectroscopy, PL and optical absorption (Davydov et al., 2002b). Fig. 2.3 shows PL spectra for InN sample grown by MBE which exhibited that the energy bandgap of InN was much lower than the earlier reported value (around 1.9 eV) (Davydov et al., 2002b). They studied in detail with high quality hexagonal InN layers grown by various epitaxy methods. From the analysis of PLE, PL and optical absorption data attained from single crystalline hexagonal InN films can be conculded that the true energy bandgap of InN might be around 0.7 eV (Davydov et al., 2002b).

The bandgap of InN films is strongly dependent on their growth conditions. Various factors that contribute to variations in bandgap include Moss–Burstein

energy shifts (Chakraborty et al., 2003), the presence of oxide precipitates (Davydov et al., 2002a), and other stoichiometry-related defects (Butcher and Tansley, 2005, Li et al., 2011). Fig. 2.4 shows that the energy bad gap values higher than 1 eV were attained for polycrystalline InN samples while the lower values were for single crystalline InN samples with a quite low carrier concentration (Butcher and Tansley, 2005). It can be concluded that the energy bandgap attained from epitaxial films depends on the carrier concentration and the obtained value is larger for polycrystalline films.

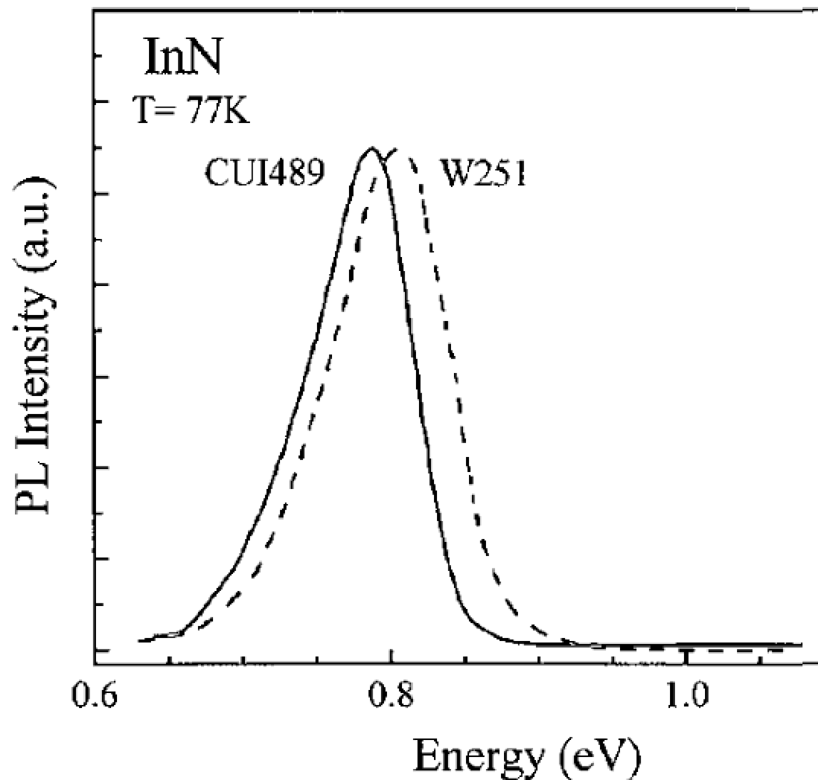

Fig. 2.3: Photoluminescence spectra for MBE grown InN. (Davydov et al., 2002b)

As Motlan *et al.* (Motlan et al., 2002) reported, the oxygen incorporation is also one of the reasons for the large energy bandgap. Consequently, the larger values might be related to the oxygen incorporation with InN samples because polycrystalline thin films may contain a high density of the oxygen atoms at the InN

grain boundaries. Davydov *et al.* (Davydov et al., 2002b) reported that the samples with energy bandgap of 1.8- 2.1 eV included more than 20 % of oxygen, relatively higher than the samples with a narrow energy bandgap. It can be presumed that oxygen is the reason for the high concentration of defects. In addition, the bandgap may increase with increasing carrier concentration, also referred to as the Moss–Burstein shift (Chakraborty et al., 2003). This effect occurs when the carrier concentration exceeds the conduction band edge density of states and the Fermi level is positioned within the conduction band.

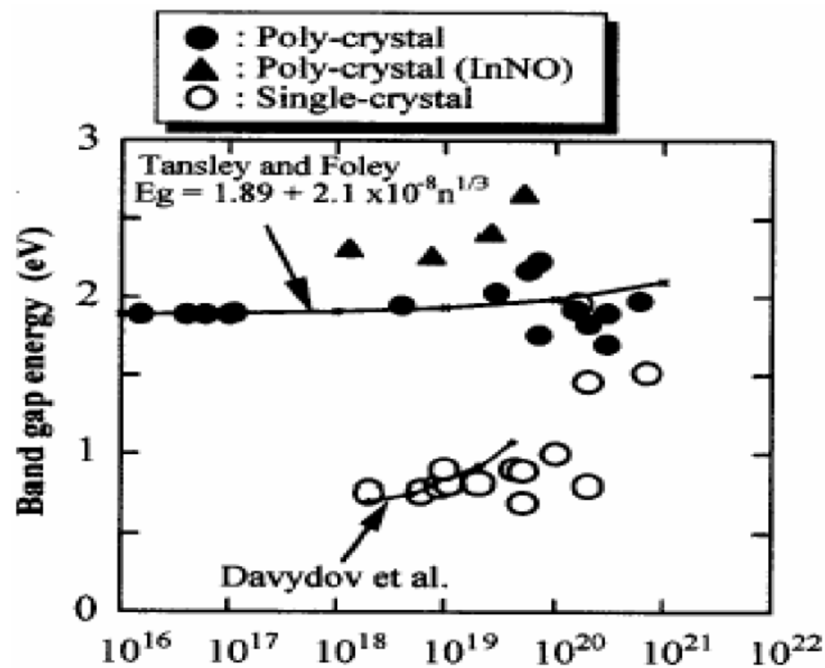

Fig. 2.4: Bandgap energy for InN films as a function of carrier concentration. (Butcher and Tansley, 2005)

2.2.3.4. Review of InN growth history

InN growth is not as easy as that of GaN and AlN. The major factors that raise the difficulty to achieve good quality single crystalline InN are low thermal stability, i.e. a decomposition temperature lower than 600 °C, higher vapor pressure of nitrogen over InN, and lack of well lattice matched substrates. The first attempt to

study on InN area began in 1938 (Juza and Hahn, 1938) when synthesized powder InN samples were examined by X-ray diffraction method in order to verify the crystallographic characteristics of this material. InN powder was obtained by Juza and Hahn (Juza and Hahn, 1938) from decomposition of $InF_6(NH_4)_3$ at temperature of 600 °C. They reported the wurtzite crystalline structure for InN with lattice parameters of c = 5.7037 Å and a = 3.5377 Å. The reported lattice constants by Juza and Hahn are in good agreement with the present measured and reported values. Research on InN material was sporadic in the years between 1938 and 1990.

In the 1974's, Trainor and Rose (Trainor and Rose, 1974) reported that the partial pressure of atomic nitrogen is a fundamental parameter describing thermal equilibrium in InN. The thermal stability research on InN samples indicates that InN decomposed in a few minutes during the annealing process at 500 °C and leaves an indium residue in N_2 (at standard pressure). However, when the InN sample was heated to 500 °C in low nitrogen pressure around 10^{-3} Torr, the InN sample did not decompose. The stability of InN samples can be attained by thermal disassociation of N_2 (Trainor and Rose, 1974). Furthermore, Trainor and Rose expressed that higher quality InN films could be attained by growing the InN films at higher temperatures around 600 °C in low pressure and lower growth rates. Marasina et al. (Marasina et al., 1977) operated chemical vapor deposition to grow InN epitaxial layers and reported that the dissociation of InN quickly occurred at 600 °C, therefore there was no deposition of InN thin films above 670 °C. Surface stabilization data of InN sample, shown in the Fig. 2.5 (Butcher and Tansley, 2005), reveals that InN can be grown at high temperature with stabilization at high nitrogen pressure.

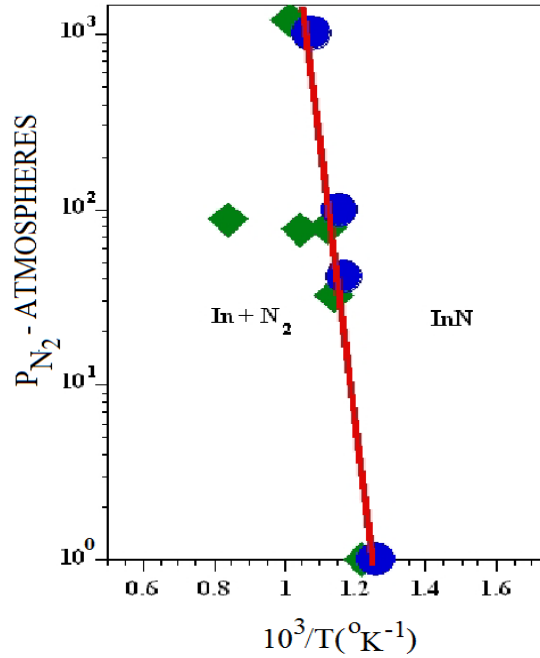

Fig. 2.5: Phase relations of InN shown by a decomposition curve separating InN and $In+N_2$ phase fields. Tetragons represent experimental conditions where metallic indium is observed. Shaded circles indicate that InN was stable. (Butcher and Tansley, 2005)

In 1990, the epitaxial single-phase InN thin films have been deposited on (001) sapphire in the temperature range of 400-600°C by microwave-excited metal organic vapor phase epitaxy (MOVPE) (Wakahara et al., 1990). It was reported that (002) InN thin films could be grown on sapphire (001) at 500 °C.

InN films have been prepared by multiple methods such as metal organic chemical vapor deposition (MOCVD), molecular beam epitaxy (MBE), atomic layer epitaxy, radio-frequency (RF) sputtering, and direct current sputtering (Cai et al., 2009, Higashiwaki and Matsui, 2003, Inushima et al., 1999, Maleyre et al., 2004, Nanishi et al., 2003, Valdueza-Felip et al., 2011). MOCVD and MBE can be used to grow single crystalline InN, but as mentioned before the epitaxial growth of InN layer under low pressure conditions such as MBE and MOCVD is difficult because the decomposition temperature of InN is low and in addition the equilibrium pressure of nitrogen increases rapidly with raising the growth temperature (Davydov and

Klochikhin, 2004). However, these methods are so costly and the size of the grown epi-layer is limited. The RF sputtering technique can be used for fabricating non-crystalline or poly-crystalline InN. Moreover, sputtering methods are suitable for deposition at room temperature. Due to its low dissociation temperature, InN film should be deposited at low temperatures to avoid N atom re-evaporation. Reactive sputtering is one of the most promising techniques of producing InN from the viewpoint of low-temperature film growth. InN layer synthesis on sapphire and glass substrates using reactive sputtering has been previously reported (da Silva et al., 2012, Inoue et al., 2004, Takai et al., 1998), and InN deposition on different Si substrate orientations and 6H-SiC substrate have been investigated. The anisotropic Si (110) surface offers a unique orientation for III-nitride films, decreasing the defect density and tensile stress for film cracking (Cordier et al., 2009). The unique characteristics of Si (110) which made it as a suitable substrate for InN based devices will be discussed later.

2.2.3.5. RF magnetron sputtering (An alternative growth technique of nanocrystalline InN films)

The deposition of thin functional films on various substrates is an important and fundamental step in different fields of modern high-technology applications. Considering the wide spectrum of applications in this area, there cannot be just one perfect deposition method in all fields. The deposition methods are commonly divided into two groups depending on whether the procedure is principally chemical or physical: Chemical Methods (Chemical Vapour Deposition, CVD), i.e. MOCVD and physical methods (Physical Vapour Deposition, PVD) such as MBE and sputtering; which both stands on depositions from vapour phase. In the present study,

the PVD category was considered. In particular, the sputtering technique is used as a suitable technique to grow large area thin film at low temperature as well as low cost. Generally, sputtering is performed at temperatures lower than 300 °C.

Sputtering means ejecting material from a target and depositing it on a substrate. Sputtering deposition is one of the most widely used technique for the thin films growth, either metal films or insulators on the substrate, as confirmed by the lots of applications of the method such as, optical coatings, solar cells, luminescence films, microelectronic applications, etc. The apparent simplicity of obtaining the large deposition area without any need for substrate motion is one of the main factors to choose this technique. Consequently, the film deposited by sputtering is uniform in thickness (Khoshman, 2005).

In general, two kinds of sputtering techniques are available for the thin film deposition; direct current (DC) and RF sputtering. DC sputtering is done with conducting materials. If the target is a nonconducting material, the positive charge is built up on the material and it stops the sputtering. RF sputtering can be done either conducting or non conducting materials. The target is the source material as a cathode electrode and substrates are placed in the anode in a vacuum chamber. Then, the chamber is pumped down to a prescribed process pressure. The sputtering process starts since a negative charge is applied to the target material causing plasma. An electric field with sufficient strength is applied between the anode and cathode to accelerate the ionized inert gas to produce highly energetic incident particles. Positive charged gas ions generated in the plasma region are attracted to the negatively biased target plate at a very high speed. This collision creates a momentum transfer and ejects atomic size particles from the target. These particles are deposited as a thin film onto the surface of the substrates. Here, magnets are used

to increase the percentage of electrons that take part in ionization of events and thereby increase the probability of electrons striking the Argon atoms, and therefore increase the ionization efficiency considerably (Sultana, 2010). The target-substrate distance can be varied which may influence the sticking coefficient of sputtered particles (Mahieu et al., 2008).

RF frequencies utilized for sputtering deposition are in the range 0.5-30 MHz. The commercial frequency which is often used is 13.56 MHz (Xiao, 2009). When a RF potential, with a large peak-to-peak voltage, is capacitively applied to an electrode, an alternating positive or negative potential appears into the surface. Since the target is capacitively placed to the plasma, there is no difference whether the targets are electrically conductive or insulating. The configuration and description of mechanism of RF magnetron sputtering system are demonstrated in the next chapter.

Sputtering deposition can be utilized to deposit thin films of compound materials by sputtering from an elemental target in a partial pressure of a reactive gas; i.e. reactive sputter deposition (RF sputtering), or by sputtering from the compound target.

2.3. Issues on the substrate for InN

Since bulk InN substrates are not available, the InN film must be grown by heteroepitaxy on different substrates such as glass, saphire and Si (Cai et al., 2009, Inoue et al., 2004). Usually, glass and sapphire are used as a substrate material for the heteroepitaxy of InN because of their wide availability, and its ease in handling and pre-growth cleaning. In addition, the hexagonal symmetry of saphire make it interesting as a substrate for InN films. However, based on outlook of device technology, sapphire has severe difficulties as a substrate material since it is difficult

to cleave. Furthermore, since the glass and sapphire substrates are not conductive, it is not possible to produce optical devices that required current to pass through the films and substrates. Consequently, it is desirable to grow the nanocrystalline InN on other semiconductor substrates.

2.3.1. Si as a suitable substrate for InN based devices

Si is a group IV element semiconductor. Currently, most of the commercial photo-electronic devices are based on Si. Si is a very interesting substrate material for the fabrication of InN-based devices because of the advantages in thermal and electrical conductivity, as well as cost-efficient substrates and accessibility in large diameters. Si has a cubic crystalline structure (Fig. 2.6) with lattice constant of 5.431 Å. Each Si atom symmetrically surrounded by 4 equally spaced neighbours (Runyan, 1965). The bandgap of Si is around 1.12 eV at room temperature. Both p-type and n-type Si substrates are available in large sizes (up to 400 mm diameter) with different doping concentrations. The various planes that pass through the crystal are described in terms of miller indices (hkl). Fig. 2.7 illustrates three common crystallographic planes which we will discuss them as different orientations of Si substrate.

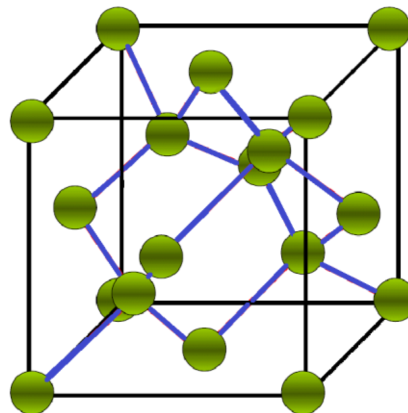

Fig. 2.6: Cubic crystalline structure of silicon.(Sze and Ng, 2006)